Dynamically Feasible Periodic Trajectories for Generic Spatial 3-DOF Cable-Suspended Parallel Robots[†]

Giovanni Mottola

Ph.D. Student
University of Bologna
Bologna, Italy 40126
Email: giovanni.mottola3@unibo.it

Clément Gosselin

Professor, Fellow of ASME
Université Laval
Québec, Canada G1V 0A6
Email: gosselin@gmc.ulaval.ca

Marco Carricato[*]

Professor
University of Bologna
Bologna, Italy 40126
Email: marco.carricato@unibo.it

ABSTRACT

Cable suspended robots may move beyond their static workspace by keeping all cables under tension, thanks to end-effector inertia forces. This may be used to extend the robot capabilities, by choosing suitable dynamical trajectories. In this paper, we consider 3D elliptical trajectories of a point-mass end-effector suspended by 3 cables from a base of generic geometry. Elliptical trajectories are the most general type of spatial sinusoidal motions. We find a range of admissible frequencies for which said trajectories are feasible; we also show that there is a special frequency which allows the robot to have arbitrarily large oscillations. The feasibility of these trajectories is verified via algebraic conditions that can be quickly verified, thus being compatible with real-time applications. By generalizing previous studies, we also study the possibility to change the frequency of oscillation: this allows the velocity at which a given ellipse is tracked to be varied, thus providing more latitude in the trajectory definition. We finally study transition trajectories to move the robot from an initial state of rest (within the static workspace) to the elliptical trajectory (and vice versa) or to connect two identical ellipses having different centres.

1 Introduction

Cable-suspended parallel robots, or CSPRs, are fully constrained if $n \geq m$, where n is the number of taut cables and m the number of degrees-of-freedom (DOFs). The usual assumption in the study of CSPRs is that they operate in static or quasi-static conditions, in the so-called Static Equilibrium Workspace (SEW), which is the volume above the robot footprint corresponding to the set of positions where the end-effector can be in static equilibrium [2]. More recent works investigated the dynamic workspace, which is the set of all end-effector poses that may be reached with positive cable tensions in a dynamic state (i. e. with nonzero velocity or acceleration [3]): this allows CSPRs to move outside the SEW, thus expanding their potential applications.

The dynamic motion of CSPRs is radically dependent on whether the robot is under or fully constrained [4–6]. As far as the former are concerned, one of the first works on this topic focused on a 2-DOF 1-cable robot moving in a plane [7]. The authors used a pendular motion to pump energy in the system and progressively increase the oscillation amplitude. This was an underactuated and thus underconstrained robot, equipped with a number of actuators smaller than the number of DOFs. Dynamic point-to-point motions of underactuated CSPRs were also studied in [8], [9], [10] and [11]. In [12], the authors present an underactuated 4-cable robot that was proven to be dynamically flat; the dynamics of a robot with a similar architecture was first studied in [13]. The dynamical trajectories of CSPRs with a passive serial support composed of rigid links were studied in [14–16].

As far as the dynamic motion of fully constrained CSPRs is concerned, reference [17] focused on a 2-DOF, fully-actuated planar robot. Here, the authors defined periodic trajectories whose feasibility can be verified by checking if the motion frequency falls within an admissible range, with-

[*]Corresponding author.

[†]A preliminary and partial version of this paper was presented at the Third International Conference on Cable-Driven Parallel Robots, August 2-4, 2017, Québec City, Canada [1].

out the necessity to integrate the inverse dynamics problem; furthermore, they found a special motion frequency, which is always within this range and is similar to the natural frequency of a pendulum. In later works, these results were applied to periodic trajectories of 3-DOF spatial point-mass robots [18] and 3-DOF planar robots [19]; later, point-to-point motions [20], [21] were also considered. Another example of dynamic modeling for parallel robots with flexible elements can be found in [22].

In this paper, we define elliptical dynamic trajectories for a spatial CSPR with 3 DOFs and a point-mass end-effector (Section 2). For these trajectories we find a special frequency, akin to the one found in [18], which allows the end-effector to achieve arbitrarily large oscillations (Section 3). We also find with a range of frequencies (Section 4) that guarantee that cable tensions remain always positive (hereafter, we will refer to this property as the *feasiblity condition*). The trajectories presented in [18], [23] and [24] are special cases of the ellipses studied here. We consider the most general location of the cable exit points on the base, even at different heights, while previous works only considered special cases: in [18] and [21], for example, the exit points are on a horizontal equilateral triangle, whereas in [23] and [24] the fixed base is a generic horizontal triangle. In [24], moreover, the authors consider spatial circular trajectories, finding a range of admissible frequencies that is strictly contained in the ampler range found in this paper (with the exception of horizontal circular trajectories, where the two ranges coincide). In Section 4 we also show the results provided by computer simulations and compare our trajectories with previous works.

We then study the possibility of changing the oscillation frequency along a given ellipse (Section 5): this is, to the best of our knowledge, a novel strategy, which was not explored in the preliminary version of this paper presented in [1].

We also consider transition motions (Subsection 6.1) to connect a state of rest to a dynamic trajectory and vice versa. As an application example, a motion of this kind can be used to safely recover a robot after a cable failure, by bringing the damaged CSPR back in the new SEW and then slowing it down [25]. In the same way, we consider transition motions that connect two identical ellipses laying on parallel planes, but having different centres (Subsection 6.2); this type of transition motion was not considered in [1] and is studied here for the first time.

2 Dynamic model

A point P moving along a trajectory Γ has a position $\mathbf{p}$ with respect to a fixed frame, defined by three sine functions:

$$\mathbf{p} = \begin{bmatrix} x \\ y \\ z \end{bmatrix} = \underbrace{\begin{bmatrix} x_C \\ y_C \\ z_C \end{bmatrix}}_{\mathbf{p}_C} + \underbrace{\begin{bmatrix} x_A \sin(\psi + \phi_x) \\ y_A \sin(\psi + \phi_y) \\ z_A \sin(\psi + \phi_z) \end{bmatrix}}_{\mathbf{p}_d} \tag{1}$$

where

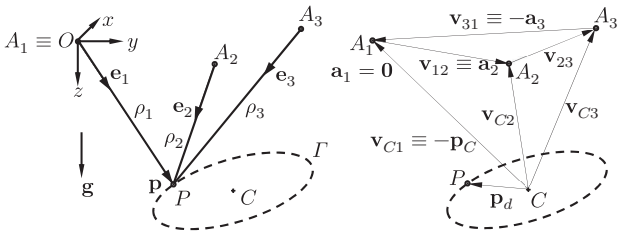

Fig. 1: (Left) Schematic of a 3-DOF spatial CSPR. (Right) Auxiliary vectors.

- x_C, y_C, z_C are the coordinates of centre C;
- x_A, y_A, z_A are the amplitudes of oscillation;
- ϕ_x, ϕ_y, ϕ_z are phase angles;
- $\psi = \psi(t)$ gives the position of P along Γ;
- $\mathbf{p}_d$ is the displacement of point P from point C.

Equation (1) represents the most general sinusoidal 3D trajectory and can be shown to be an ellipse (or an elliptical arc); see Appendix A. This trajectory generalizes the periodic trajectories presented in [1], since here angle $\psi(t)$ is a general function of time. Special cases include circles and line segments, either horizontal, vertical or oblique (cases dealt with in [18], [23] and [24]). It should be noted that general elliptical trajectories were first considered in [26]; however, the authors did not consider phase angles nor provided conditions for these trajectories to be feasible.

We now consider a spatial CSPR whose end-effector is modeled as a point-mass P. The positions of P and of the cable exit points A_i are respectively $\mathbf{p} = [x, y, z]^T$ and $\mathbf{a}_i = [x_{ai}, y_{ai}, z_{ai}]^T$, for $i = 1, 2, 3$ (in Fig. 1, without loss of generality, we set $O \equiv A_1$). For future convenience, we define

$$\mathbf{v}_{Ci} = [x_{Cai}, y_{Cai}, z_{Cai}]^T = \mathbf{a}_i - \mathbf{p}_C \quad (i \in 1, 2, 3) \tag{2}$$

$$\mathbf{v}_{jk} = [x_{ajk}, y_{ajk}, z_{ajk}]^T = \mathbf{a}_k - \mathbf{a}_j \quad (j, k \in 1, 2, 3) \tag{3}$$

$$\boldsymbol{\lambda}_i = [\lambda_{xi}, \lambda_{yi}, \lambda_{zi}]^T = \mathbf{v}_{Cj} \times \mathbf{v}_{Ck} \tag{4}$$

These are the position vectors $\mathbf{v}_{Ci}$ from C to A_i and $\mathbf{v}_{jk}$ from A_j to A_k, while $\boldsymbol{\lambda}_i$ is their cross product; in eq. (4), the indices j and k depend on i as follows:

$$\begin{cases} i = 1 \rightarrow j = 3, k = 2 \\ i = 2 \rightarrow j = 1, k = 3 \\ i = 3 \rightarrow j = 2, k = 1 \end{cases} \tag{5}$$

so for example $\boldsymbol{\lambda}_1 = \mathbf{v}_{C3} \times \mathbf{v}_{C2}$. We also define lengths $\rho_i = \|\mathbf{p} - \mathbf{a}_i\|$ and unit vectors $\mathbf{e}_i = (\mathbf{p} - \mathbf{a}_i)/\rho_i$ for $i \in \{1, 2, 3\}$.

The end-effector is subjected to the gravitational force $m\mathbf{g}$ (here, we take a reference frame with the z axis pointing downwards, so that $\mathbf{g} = [0, 0, g]^T$), the cable tensions $\tau_i \mathbf{e}_i$ and the inertial force $-m\ddot{\mathbf{p}}$. We assume that the cables are massless and infinitely stiff. The equilibrium equation is then

$$m\mathbf{g} - \sum_{i=1}^{3} \tau_i \mathbf{e}_i = m\ddot{\mathbf{p}} \tag{6}$$

(as per Newton's dynamic equations) which we rewrite as

$$m(\mathbf{g}-\ddot{\mathbf{p}}) = \mathbf{M}[\tau_1,\tau_2,\tau_3]^T \tag{7}$$

where $\mathbf{M} = [\mathbf{e}_1,\mathbf{e}_2,\mathbf{e}_3]$. It may be proven that $\det\mathbf{M} < 0$, as long as P moves below the plane Π that passes through points A_i and the latter are numbered in clockwise order (as seen from above). Plane Π has equation

$$ax + by + cz + d = 0 \tag{8}$$

with coefficients a, b, c, d depending on points A_i as follows:

$$\begin{aligned} a &= \begin{vmatrix} 1 & y_{a1} & z_{a1} \\ 1 & y_{a2} & z_{a2} \\ 1 & y_{a3} & z_{a3} \end{vmatrix}, \quad b = \begin{vmatrix} x_{a1} & 1 & z_{a1} \\ x_{a2} & 1 & z_{a2} \\ x_{a3} & 1 & z_{a3} \end{vmatrix} \\ c &= \begin{vmatrix} x_{a1} & y_{a1} & 1 \\ x_{a2} & y_{a2} & 1 \\ x_{a3} & y_{a3} & 1 \end{vmatrix}, \quad d = -\begin{vmatrix} x_{a1} & y_{a1} & z_{a1} \\ x_{a2} & y_{a2} & z_{a2} \\ x_{a3} & y_{a3} & z_{a3} \end{vmatrix} \end{aligned} \tag{9}$$

We note here that c is twice the (signed) area of the triangle T_{xy} defined by points (x_{ai}, y_{ai}); having numbered points A_i in clockwise order, this signed area is negative and so $c < 0$.

If P has to remain below Π, trajectory Γ must not intersect Π. To check this condition we substitute eq. (1) into eq. (8) and obtain

$$Q_0 + Q_s \sin(\psi) + Q_c \cos(\psi) = 0 \tag{10}$$

where Q_0, Q_s and Q_c are as follows:

$$\begin{aligned} Q_0 &= ax_C + by_C + cz_C + d \\ Q_s &= ax_A \cos\phi_x + by_A \cos\phi_y + cz_A \cos\phi_z \\ Q_c &= ax_A \sin\phi_x + by_A \sin\phi_y + cz_A \sin\phi_z \end{aligned} \tag{11}$$

Equation (10) can be solved by the tangent half-angle method, having set $t_n = \tan(\psi/2)$. In this way, we find a quadratic equation in t_n, which must have no solutions when Γ does not intersect Π. Its discriminant must then be negative, so

$$4(Q_s^2 + Q_c^2 - Q_0^2) < 0 \tag{12}$$

This is a condition for feasibility that can easily be checked.

If $\det\mathbf{M} < 0$, $\tau_i > 0$ (see [18], eqs. (17)-(19)) if and only if

$$\mu_i = \left[\mathbf{p}\times(\mathbf{a}_k - \mathbf{a}_j) + \mathbf{a}_k \times \mathbf{a}_j\right]^T (\ddot{\mathbf{p}} - \mathbf{g}) > 0 \tag{13}$$

where again j and k depend on i as per eq. (5).

3 Natural frequency

The authors of Refs. [17] and [18] found that arbitrarily large motions may be followed, while keeping positive tensions, if the robot moves with a special frequency $\omega_n = \sqrt{g/z_C}$, where z_C is the z coordinate of centre C. We now show that there is a similar frequency for the trajectories studied in this paper.

In analogy to [21], we suppose that tensions τ_i are kept proportional to cable lengths ρ_i, which can be done by suitably controlling the actuators. Equation (6) becomes

$$m\mathbf{g} - \sum_{i=1}^{3} k_i(\mathbf{p} - \mathbf{a}_i) = m\ddot{\mathbf{p}} \tag{14}$$

where k_i is a virtual cable stiffness. We rewrite eq. (1) as

$$\mathbf{p} = \mathbf{p}_C + \mathbf{c}\cos(\omega t) + \mathbf{s}\sin(\omega t) = \mathbf{p}_C + \mathbf{p}_d \tag{15}$$

where $\omega t = \psi$ and ω being the motion frequency. Substituting eq. (15) in eq. (14) we find

$$m[\mathbf{g} + \omega^2(\mathbf{p} - \mathbf{p}_C)] = \sum_{i=1}^{3} k_i(\mathbf{p} - \mathbf{a}_i) \tag{16}$$

We define ω_n as the natural frequency of the second order ODE in eq. (14), namely $m\omega_n^2 = k_1 + k_2 + k_3 = K$. If we set $\omega = \omega_n$ in eq. (16), the terms in p cancel out:

$$m\mathbf{g} - K\mathbf{p}_C = -\sum_{i=1}^{3} k_i \mathbf{a}_i \tag{17}$$

If $k_i > 0$ and eq. (17) holds, the cable tensions $\tau_i = k_i\rho_i$ are positive, since clearly $\rho_i > 0$. The trajectory may then be realized with $\tau_i = k_i\rho_i$ if and only if eq. (17) is satisfied: this, together with the condition $k_1 + k_2 + k_3 = K$, gives a linear system of equations in the unknowns k_i, which has solution

$$\begin{bmatrix} k_1 & k_2 & k_3 \end{bmatrix} = -\frac{mg}{Q_0}\begin{bmatrix} \lambda_{z1} & \lambda_{z2} & \lambda_{z3} \end{bmatrix} \tag{18}$$

with Q_0 defined in eq. (11). The natural frequency ω_n is then

$$\omega_n = \sqrt{\frac{K}{m}} = \sqrt{-\frac{g(\lambda_{z1} + \lambda_{z2} + \lambda_{z3})}{Q_0}} = \sqrt{\frac{gc}{Q_0}} \tag{19}$$

We know that $c < 0$ (cf. Section 2) and $\omega_n \in \mathbb{R}_{>0}$, so it must be $Q_0 < 0$. It then follows from eq. (18) that, for the k_i's to be positive, λ_{zi} must be positive too: it may be shown that this implies that the projection of point C on plane $x - y$ must be within the triangle T_{xy} (cf. Section 2). This condition and the requirement that Γ must be below Π imply that C has to

be within the SEW (which is the set of all points within the convex hull of the A_i or below this region).

These results expand those presented in [18], [23] and [24], where the authors assumed points A_i to have the same z coordinate and Γ to be a circle.

4 Generic frequency

It is also possible to have periodic motions along a trajectory Γ with frequencies ω different from the ω_n given in eq. (19). To study this general case, we substitute eq. (1) into eq. (13). Each μ_i can now be written as

$$\mu_i = C_i \cos(\psi) + D_i \sin(\psi) + E_i \tag{20}$$

with

$$\begin{aligned} C_i &= C_{i,a}\ddot{\psi} + C_{i,v}\dot{\psi}^2 + C_{i,c} \\ D_i &= D_{i,a}\ddot{\psi} + D_{i,v}\dot{\psi}^2 + D_{i,c} \\ E_i &= E_{i,a}\ddot{\psi} + E_{i,c} \end{aligned} \tag{21}$$

having defined the following auxiliary parameters:

$$\begin{aligned} &\phi_{xy} = \phi_x - \phi_y && \phi_{yz} = \phi_y - \phi_z && \phi_{zx} = \phi_z - \phi_x \\ &\mathbf{n}_e = \begin{bmatrix} y_A z_A \sin\phi_{yz} & z_A x_A \sin\phi_{zx} & x_A y_A \sin\phi_{xy} \end{bmatrix} \\ &\mathbf{p}_{d,c} = \begin{bmatrix} x_A \cos\phi_x & y_A \cos\phi_y & z_A \cos\phi_z \end{bmatrix} \\ &\mathbf{p}_{d,s} = \begin{bmatrix} x_A \sin\phi_x & y_A \sin\phi_y & z_A \sin\phi_z \end{bmatrix} \\ &C_{i,a} = -\boldsymbol{\lambda}_i \cdot \mathbf{p}_{d,c}, && D_{i,a} = \boldsymbol{\lambda}_i \cdot \mathbf{p}_{d,s} \\ &C_{i,v} = D_{i,a}, && D_{i,v} = -C_{i,a} \\ &C_{i,c} = \mathbf{g} \cdot (\mathbf{p}_{d,s} \times \mathbf{v}_{kj}), && D_{i,c} = \mathbf{g} \cdot (\mathbf{p}_{d,c} \times \mathbf{v}_{kj}) \\ &E_{i,a} = \mathbf{v}_{kj} \cdot \mathbf{n}_e, && E_{i,c} = g\lambda_{zi} \end{aligned} \tag{22}$$

Here, j and k depend on i as per eq. (5) and $\mathbf{n}_e$ is a vector normal to the plane of the ellipse.

If $\psi = \omega t$, then $\dot{\psi} = \omega$, $\ddot{\psi} = 0$ and $C_i = C_{i,v}\omega^2 + C_{i,c}, D_i = D_{i,v}\omega^2 + D_{i,c}, E_i = E_{i,c}$. In this case, coefficients C_i, D_i, E_i are constant, once the trajectory Γ has been chosen: C_i and D_i are linear functions of ω^2, while E_i only depends on g and the position of C. Equation (20) is analogous to one reported in [18] for the special case of circular trajectories (either horizontal or vertical). The definitions in eq. (22) generalize the ones that we first provided in [1] for the case when $\psi(t)$ is a general function of time.

The extreme values of eq. (20) are

$$\mu_{i,1} = \sqrt{C_i^2 + D_i^2} + E_i, \quad \mu_{i,2} = -\sqrt{C_i^2 + D_i^2} + E_i \tag{23}$$

If both the extrema are positive, then μ_i is guaranteed to be positive. From eq. (23) it's clear that, if $E_i = \lambda_{zi} g < 0$, then $\mu_{i,2} < 0$, so μ_i will be negative at some point for any value of ω. We then require $\lambda_{zi} > 0$ which is the condition already found in Section 3.

Since $\mu_{i,2} < \mu_{i,1}$, it is sufficient to check that $\mu_{i,2} > 0$, so that $E_i > \sqrt{C_i^2 + D_i^2}$. Both sides of this equation are positive, so we may square them to find $E_i^2 > C_i^2 + D_i^2$. After inserting the definitions of C_i, D_i and E_i in eq. (21), we obtain a fourth degree inequality:

$$\mu_{i,2} > 0 \quad \Leftrightarrow \quad \alpha_i \omega^4 + 2\beta_i \omega^2 + \gamma_i < 0 \tag{24}$$

with

$$\begin{aligned} \alpha_i &= C_{i,v}^2 + D_{i,v}^2 \\ \beta_i &= C_{i,c} C_{i,v} + D_{i,c} D_{i,v} \\ \gamma_i &= C_{i,c}^2 + D_{i,c}^2 - E_{i,c}^2 \end{aligned} \tag{25}$$

The authors of [18, 23, 24] found ranges of feasible values for ω that guarantee the feasibility of a given circular trajectory, assuming points A_i to be at the same height. We can assume that a similar range may be defined in our broader case, if there is at least one value of ω satisfying eq. (25); ω_n is indeed one such value, since in this case the trajectory is feasible (see Section 3).

To find the aforementioned range, we set $\omega^2 = w$ in eq. (24), thus obtaining a quadratic inequality in w, namely $\alpha_i w^2 + 2\beta_i w + \gamma_i < 0$. We note that, by the definition in eq. (25), $\alpha_i \geq 0$, so $\alpha_i w^2 + 2\beta_i w + \gamma_i = \zeta$ defines a convex parabola in the $w - \zeta$ plane for positive α_i; the degenerate case $\alpha_i = 0$ will be considered later.

Depending on the sign of $\Delta_i = \beta_i^2 - \alpha_i \gamma_i$, we have 3 cases:

(a) $\Delta_i > 0$: there are two values $w_{i,min}$ and $w_{i,max}$ (which in general will be different for the three cables) such that, if $w \in \left]w_{i,min}, w_{i,max}\right[$, then $\alpha_i w^2 + 2\beta_i w + \gamma_i < 0$;
(b) $\Delta_i = 0$: the inequality has a single solution, i.e. $\omega = \omega_n$;
(c) $\Delta_i < 0$: the inequality has no solutions.

We know that inequality (24) has at least one solution, $\omega = \omega_n$, as long as the trajectory Γ respects the conditions found in Section 3 (C must be in the SEW and Γ is below Π): under these conditions, the three Δ_i's must be positive (case (a)).

When $\Delta_i > 0$, the values $w_{i,min}$ and $w_{i,max}$ are given by

$$w_{i,min} = \frac{-\beta_i - \sqrt{\Delta_i}}{\alpha_i}, \quad w_{i,max} = \frac{-\beta_i + \sqrt{\Delta_i}}{\alpha_i} \tag{26}$$

Recalling that $w = \omega^2 > 0$, we can have the following cases:

(A) If $w_{i,min}$ and $w_{i,max}$ are ≤ 0, no value of ω is feasible;
(B) If $w_{i,min} \leq 0$ and $w_{i,max} > 0$, the range of ω satisfying eq. (24) is $\left]0, \sqrt{w_{i,max}}\right]$;
(C) If $w_{i,min}$ and $w_{i,max}$ are positive, the condition on ω is $\omega \in \left[\sqrt{w_{i,min}}, \sqrt{w_{i,max}}\right]$.

We finally define three ranges for ω, one for each cable: these ranges are either like $\left]0, \sqrt{w_{i,max}}\right]$ (case (B)) or like $\left[\sqrt{w_{i,min}}, \sqrt{w_{i,max}}\right]$ (case (C)), depending on the sign of

$w_{i,min}$. We can now define the extremes of the range for ω that ensure positive cable tensions:

$$\begin{aligned} \omega_{min} &= \sqrt{\max\left\{\max\left\{w_{i,min}\right\},0\right\}} \quad , \\ \omega_{max} &= \sqrt{\min\left\{w_{i,max}\right\}} \end{aligned} \tag{27}$$

Under the conditions in Section 3 (namely, C is in the SEW and trajectory Γ is below plane Π), the condition for feasibility is $\omega_{min} \leq \omega \leq \omega_{max}$. Note that ω_{min} and ω_{max} are defined by explicit algebraic formulae and, thus, easy to calculate.

From eq. (27), we see that ω_{min} might be zero. For ω sufficiently close to zero, the end effector moves quasi-statically, so the inertial force is negligible: ω_{min} is then zero if and only if Γ is completely within the SEW (we discard the case $\omega = 0$, since in this case the robot does not move).

We note that if $\omega = \omega_{min}$ or $\omega = \omega_{max}$, one or more of the cable tensions has a minimum value equal to zero along the trajectory. The conditions above are therefore strict, while those found in [24] are only sufficient (but not strictly necessary): the range for ω that we found is therefore larger than that given in [24].

An interesting particular case is when $z_{a,i} = z_a\,(i \in 1,2,3)$, so that cable exit points A_i are all at the same height z_a: in this case eq. (9) gives $a = b = 0, d = -c \cdot z_a$, so $Q_0 = c(z_C - z_a)$ and, from eq. (19), $\omega_n = \sqrt{g/(z_C - z_a)}$ [25]. For $\omega = \omega_n$, we obtain (after some simplification) $\mu_i = \lambda_{zi}\left[g + z_A\omega_n^2 \sin(\omega_n t + \phi_z)\right]$: this implies $\mu_i \geq 0$ as long as $g \geq z_A\omega_n^2 = \max\{|\ddot{z}|\}$. This condition means that the maximum acceleration along z cannot be greater than g, as expected, and is automatically fulfilled if Γ is below Π.

Finally, we address the degenerate case for which $\alpha_i = 0$ for some i. Since α_i is a sum of squares, it can be zero only if both squares are zero, namely $C_{i,v} = D_{i,v} = 0$. This is a linear homogeneous system of two equations in the three unknowns x_A, y_A, z_A: its solutions are of the form

$$\begin{bmatrix} x_A \\ y_A \\ z_A \end{bmatrix} = f_1 \begin{bmatrix} \lambda_{yi}\lambda_{zi}\sin(\phi_{yz}) \\ \lambda_{zi}\lambda_{xi}\sin(\phi_{zx}) \\ \lambda_{xi}\lambda_{yi}\sin(\phi_{xy}) \end{bmatrix} \tag{28}$$

where $f_1 \in \mathbb{R}_{>0}$ is any positive scalar. Substituting eq. (28) in eq. (25), we find that $\beta_i = 0$, too; then, in order to satisfy the inequality in (24), the only condition to check is $\gamma_i < 0$, which no longer depends on ω. It can also be proved that $\alpha_i = 0$ if and only if Γ lies on the plane through C, A_j and A_k, with $j, k \neq i$.

Some simulations were also performed to verify the theoretical findings presented above.

Figs. 2 and 3 refer to a periodic motion along an elliptical trajectory. The method described in [24] gives a range of admissible motion frequencies comprised between $\omega'_{min} = 1.548$ and $\omega'_{max} = 2.55$. By our approach we find that the actual endpoints of the admissible range, as defined in eq. (27), are $\omega_{min} = 1.387$ and $\omega_{max} = 2.75$. As expected, the first range is smaller and strictly contained in the second.

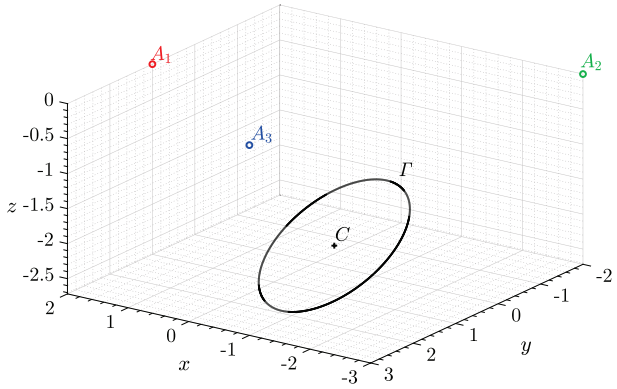

Fig. 2: An elliptical trajectory Γ with $\mathbf{p}_C = [-1,1,2]^T, a_1 = [2,1,0]^T, a_2 = [-3,-2,0]^T, a_3 = [-1,3,0]^T$ and lying on a plane normal to $\mathbf{n}_e = [1,2,3]^T$. In this special case, the cable exit points A_i are all at the same height and the trajectory is a circle with radius $R = 1.2$. The length units are arbitrary.

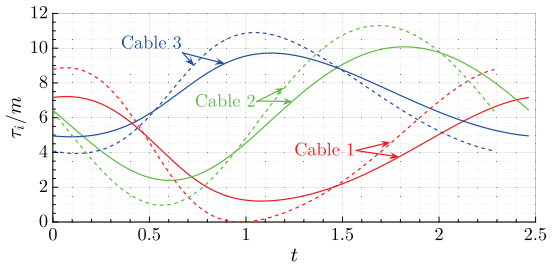

Fig. 3: The cable tensions divided by the mass of the end effector, given by a simplified model with stiff massless cables. For each cable, the solid line corresponds to $\omega = \omega'_{max}$, while the dashed line corresponds to $\omega = \omega_{max} > \omega'_{max}$.

Fig. 3 shows a plot of the cable tensions τ_i divided by the end-effector m as a function of time. Here, the continuous lines correspond to $\omega = \omega'_{max}$, while the dashed ones are for $\omega = \omega_{max}$; this latter case corresponds to a strict limit on the value of ω, so one cable tension reaches zero at one point (while remaining positive otherwise). By taking $\omega = \omega'_{max}$, instead, the motion period is longer (since $\omega'_{max} < \omega_{max}$) and tensions do not reach the zero value, which shows that the conditions given in [24] are not strict.

5 Variable frequency

To further generalize our previous work in [1], we now study the possibility of varying the velocity by which the robot moves along an assigned trajectory: we consider the case where the angle ψ in eq. (1) is a general function of time. In this case, coefficients C_i, D_i and E_i in eq. (20) are no longer constant. To find the minimum of μ_i, we must differentiate eq. (20) with respect to time and set the result to zero. The exact solution of this problem is however complex and (seemingly) unsuitable for real-time applications.

A simpler alternative is to find a lower bound for the

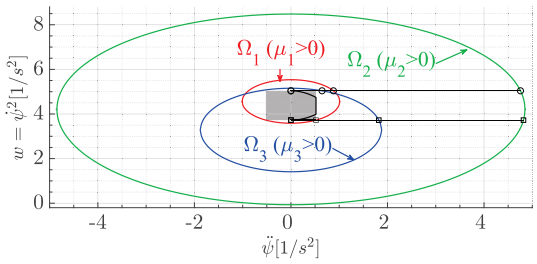

Fig. 4: Plane $\ddot{\psi} - \psi^2$ with the three ellipses Ω_i, rectangle R_ψ (in gray) and curve Γ_ψ (black line). Notice how $R_\psi \in \Omega_1 \cap \Omega_2 \cap \Omega_3$ and $\Gamma_\psi \in R_\psi$.

extrema of μ_i by interval analysis. If the values of C_i, D_i are kept fixed for assigned values of $\dot{\psi}$ and $\ddot{\psi}$ while varying ψ in eq. (20), we can use the same approach described in Section 4 to find the minimum of μ_i. It is thus found that

$$\min\{\mu_i\} = -\sqrt{C_i^2 + D_i^2} + E_i \tag{29}$$

A sufficient condition for having $\mu_i > 0$

$$E_i > \sqrt{C_i^2 + D_i^2} \tag{30}$$

If we assume $E_i > 0$ (this assumption will be verified later on), we can square both sides and obtain again three bi-quadratic inequalities, expressed as $\alpha_i \psi^4 + 2\beta_i \psi^2 + \gamma_i' < 0$. The coefficients α_i and β_i are the same as in eq. (25), while $\gamma_i' = \ddot{\psi}^2 \gamma_{i,\ddot{\psi}} + \gamma_i$ and $\gamma_{i,\ddot{\psi}} = C_{i,v}^2 + D_{i,v}^2 - E_{i,a}^2$.

If we set $w = \psi^2$, the parabola defined in the $w - \zeta$ plane by $\alpha_i w^2 + 2\beta_i w + \gamma_i' = \zeta$ shifts along the ζ axis as $\ddot{\psi}$ varies, since the only coefficient that depends on $\ddot{\psi}$ is the constant term. The parabola is convex (see Section 4), so the range of w satisfying $\alpha_i w^2 + 2\beta_i w + \gamma_i \le 0$ is given by $[w_{i,min}, w_{i,max}]$, with $w_{i,min}$ and $w_{i,max}$ given by the points of intersection of the parabola with the w axis; the centre of this range is $w_{i,c} = -\beta_i/\alpha_i$. Changing $\ddot{\psi}$ leaves the middle point $w_{i,c}$ unaltered, but the width of the admissible range varies, since $\Delta_i' = \beta_i^2 - \alpha_i \gamma_i' = \beta_i^2 - \alpha_i(\ddot{\psi}^2 \gamma_{i,\ddot{\psi}} + \gamma_i) = \Delta_i - \alpha_i \ddot{\psi}^2 \gamma_{i,\ddot{\psi}}$ changes.

It may be proven that, if C is in the SEW (so $\Delta_i > 0$), then $\gamma_{i,\ddot{\psi}} > 0$ (see Appendix B). The figure Ω_i defined by all points in the $\ddot{\psi} - w$ plane satisfying $\alpha_i w^2 + 2\beta_i w + \gamma_i'(\ddot{\psi}) \le 0$ is then an ellipse, symmetrical with respect to the w axis (γ_i' only depends on $\ddot{\psi}^2$; see Fig. 4). It can also be proved that, for every point in Ω_i, $E_i > 0$, as required (see Appendix B). We now look for a motion law $\psi(t)$ that allows us to change the motion frequency along Γ from ω_I to ω_F. Here, ω_I and ω_F must be in the admissible range for ω defined in Section 4. We set $\dot{\psi} = U(t)$ and $\ddot{\psi} = V(t) = dU/dt$, where $U(t)$ is a function of class C^1 defined for $t \in [0, T]$ and T is the transition time from ω_I to ω_F. We impose the boundary conditions $U(0) = \omega_I$, $U(T) = \omega_F$ and $V(0) = V(1) = 0$ and we also require $V(t) \ge 0$ for $t \in [0, T]$, so that the function $U(t)$ is monotonically increasing.

The extreme values of $\dot{\psi}$ are ω_I and ω_F (since U is monotonic), while the extreme value of $|\ddot{\psi}|$ is $\ddot{\psi}_e = \max|V(t)|$. As a consequence, the curve Γ_ψ described in the plane $\ddot{\psi} - \psi^2$ during the transition is then entirely contained in a rectangle R_ψ defined by $w_I = \omega_I^2 < w < w_F = \omega_F^2$ and $|\ddot{\psi}| < \ddot{\psi}_e$ (Fig. 4).

We then have only to find the minimum time T such that $R_\psi \in \Omega_1 \cap \Omega_2 \cap \Omega_3$. Since the ellipses Ω_i's are convex, we only have to check that the corners of R_ψ are within all three Ω_i's. Moreover, since the latter are symmetric w.r.t. the w axis, we may check only the two corners of R_ψ with $\ddot{\psi} > 0$, that is, those with coordinates $(\ddot{\psi}_e, w_I)$ and $(\ddot{\psi}_e, w_F)$.

The point $(\ddot{\psi}_{I,\partial\Omega_i}, w_I)$ on the boundary $\partial\Omega_i$ can be found analytically by solving $\alpha_i w_I^2 + 2\beta_i w_I + \gamma_i'(\ddot{\psi}_{I,\partial\Omega_i}) = 0$: see Fig. 4, where such points have been marked by squares. Equivalent results (with w_F in place of w_I) can be found for the points $(\ddot{\psi}_{F,\partial\Omega_i}, w_F)$, marked by circles in Fig. 4. Finally, we define

$$\begin{aligned}\ddot{\psi}_{max} = \min\{&\ddot{\psi}_{I,\partial\Omega_1}, \ddot{\psi}_{I,\partial\Omega_2}, \ddot{\psi}_{I,\partial\Omega_3}, \\ &\ddot{\psi}_{F,\partial\Omega_1}, \ddot{\psi}_{F,\partial\Omega_2}, \ddot{\psi}_{F,\partial\Omega_3}\}\end{aligned} \tag{31}$$

If $\ddot{\psi}_e < \ddot{\psi}_{max}$, R_ψ is contained within all Ω_i's and the transition motion is feasible.

The only issue that is left is to pick a suitable motion law $U(t)$ and find the minimum transition time T. $U(t)$ has to be of class C^1; moreover, it would be convenient to choose $U(t)$ such that its second derivative $W(t) = d^2U/dt^2$ quickly reaches its maximum value and then remains constant for most of the motion. In this way, the curve Γ_ψ closely follows the borders of rectangle R_ψ, the acceleration is only slightly under the maximum prescribed values $\ddot{\psi}_{max}$ and the transition time is reduced: a linear motion law with parabolic blends appears to be suitable.

6 Transition trajectories

6.1 Variable amplitudes

The sinusoidal trajectory defined in eq. (1) has velocity $\mathbf{p}$ and acceleration $\mathbf{p}$ that are nonzero at all points (if $\omega \neq 0$), so the robot cannot be in a state of rest. For practical applications, the robot has to reach a dynamic state starting from rest and vice versa. For this purpose, we define transition motions as follows:

$$\mathbf{p} = \mathbf{p}_C + U(\xi)\mathbf{p}_d \tag{32}$$

where $\mathbf{p}_C$ and $\mathbf{p}_d$ are defined as in Section 2 (here again $\psi = \omega t$, with ω being a constant frequency). $U(\xi)$ is a function of class C^2 and depends on the adimensional variable $\xi = t/T$ (with T being the duration of the transition). Equation (32) is a generalization of eq. (1); the former degenerates in the latter when $U(\xi) = 1$ (constant amplitudes).

We introduce the derivatives $V(\xi) = dU/d\xi$ and $W(\xi) =$

$d^2U/d\xi^2$ and set the boundary conditions:

$$\begin{cases} U(0) = 0, & U(1) = 1 \\ V(0) = 0, & V(1) = 0 \\ W(0) = 0, & W(1) = 0 \end{cases} \tag{33}$$

We require $U(\xi)$ to be monotonically increasing, so $V(\xi)$ is always positive. With these conditions, the robot starts moving from position $\mathbf{p} = \mathbf{p}_C$ at $t = 0$, when it is at rest ($\dot{\mathbf{p}} = \ddot{\mathbf{p}} = \mathbf{0}$); then the amplitudes of motion along the coordinate axes grow until at time $t = T$ the trajectory can be blended with the periodic elliptical motion (ellipse Γ).

With another choice of boundary conditions, eq. (32) can be similarly used to slow down a robot moving on an ellipse Γ (defined as in eq. (1)) until it stops in the centre C of the ellipse. Moreover, it can be used to connect two ellipses Γ_s and Γ_f, where Γ_f is Γ_s "scaled" by a factor F, so the two ellipses have the same centre C and the same phase angles, but different amplitudes ($x_{Af} = F x_{As}$ and so on): for this case, we simply set $U(1) = F \cdot U(0)$. For the sake of brevity, we will only study the first case, with $U(0) = 0$, $U(1) = 1$; the other cases can be studied in a similar way.

Substituting eq. (32) in eq. (13), we obtain

$$\begin{aligned} \mu_i = q_{i,W} \frac{W(\xi)}{T^2} + q_{i,V} \frac{V(\xi)}{T} + q_{i,UV} \frac{U(\xi)V(\xi)}{T} \\ + \underbrace{q_{i,U} U(\xi) + E_i}_{\mu_{i,0}} \end{aligned} \tag{34}$$

with

$$\begin{aligned} q_{i,W} &= -\boldsymbol{\lambda}_i \cdot \mathbf{p}_d \\ q_{i,V} &= -2\boldsymbol{\lambda}_i \cdot \dot{\mathbf{p}}_d \\ q_{i,UV} &= 2\omega E_{i,a} \\ q_{i,U} &= C_i \cos(\omega t) + D_i \sin(\omega t) \end{aligned} \tag{35}$$

where C_i, D_i are as in eq. (21) and $E_{i,a}$ is defined in eq. (22).

To see whether the so-defined motion is feasible, we consider $T \to \infty$, so that (from eq. (34)) $\mu_i \to \mu_{i,0} = q_{i,U} U(\xi) + E_i$.

The minimum value of $q_{i,U}$ is $q_{i,U,min} = -\sqrt{C_i^2 + D_i^2}$, while the maximum value of U (for $\xi \in [0,1]$) is $U_{max} = 1$, since U is monotonically increasing from $U(0) = 0$ to $U(1) = 1$. A lower bound for the minimum value of $\mu_{i,0}$ is then $\mu_{i,0,LB} = q_{i,U,min} U_{max} + E_i = -\sqrt{C_i^2 + D_i^2} + E_i = \mu_{i,2}$: this is the minimum value defined in eq. (23), which is positive if the target trajectory Γ is feasible (see Section 4). Therefore, the transition motion is feasible if we take T to be very large, since in this case $\mu_i \approx \mu_{i,0} > \mu_{i,0,LB} > 0$.

It would be clearly of practical interest to know the minimum value of T that guarantees positive cable tensions. In order to find it, we could set the time-derivative of eq. (34) to zero: we would then find the extrema $\mu_{i,min}$ and $\mu_{i,max}$ of μ_i. Then, we should search for the minimum T such that $\mu_{i,min} > 0$ (for $i = 1, 2, 3$). This method however leads to complex equations that must be solved numerically; thus, it does not appear suitable for real-time problems.

We adopt a simpler alternative, finding a lower bound for the minimum value of μ_i. The extreme values of $q_{i,W}$ and $q_{i,V}$, which are functions of time, are (see Appendix C)

$$\begin{aligned} q_{i,W,e} &= \max\left\{\left|q_{i,W}\right|\right\} = \|\boldsymbol{\Phi}_i\| \\ q_{i,V,e} &= \max\left\{\left|q_{i,V}\right|\right\} = 2\omega\|\boldsymbol{\Phi}_i\| \end{aligned} \tag{36}$$

with

$$\|\boldsymbol{\Phi}_i\| = \sqrt{C_{i,a}^2 + D_{i,a}^2} \tag{37}$$

We also define $V_e = \max\{|V(\xi)|\}$, $W_e = \max\{|W(\xi)|\}$ and $(UV)_e = \max\{|U(\xi) \cdot V(\xi)|\}$. Here, all extrema are those found in the interval $\xi \in [0,1]$ and depend on the chosen function $U(\xi)$. A lower bound for eq. (34) is then

$$\mu_{i,LB} = -q_{i,W,e} \frac{W_e}{T^2} - q_{i,V,e} \frac{V_e}{T} + q_{i,UV} \frac{(UV)_e}{T} + \mu_{i,0,LB} \tag{38}$$

if $q_{i,UV} < 0$, and

$$\mu_{i,LB} = -q_{i,W,e} \frac{W_e}{T^2} - q_{i,V,e} \frac{V_e}{T} + \mu_{i,0,LB} \tag{39}$$

otherwise. If we set T such that $\mu_{i,LB} > 0$, then $\mu_i \geq \mu_{i,LB} > 0$ and the trajectory is feasible. We can now express $\mu_{i,LB}$ as a function of T:

$$\mu_{i,LB}(T) = \frac{\mu_{i,c} + \mu_{i,T} T + \mu_{i,T^2} T^2}{T^2} = \frac{M_i(T)}{T^2} \leq \mu_i \tag{40}$$

with

$$\begin{aligned} \mu_{i,c} &= -q_{i,W,e} W_e \\ \mu_{i,T} &= \begin{cases} -q_{i,V,e} V_e + q_{i,UV} (UV)_e & q_{i,UV} < 0 \\ -q_{i,V,e} V_e & q_{i,UV} \geq 0 \end{cases} \\ \mu_{i,T^2} &= \mu_{i,0,LB} \end{aligned} \tag{41}$$

We have already shown that, if the starting trajectory Γ (defined by eq. (32) with $U(\xi) = 1$) is feasible, then $\mu_{i,T^2} = \mu_{i,0,LB} = \mu_{i,2} > 0$. From this we find that, if $\mu_{i,LB}(T) = 0$ (which implies $M_i(T) = 0$) has solutions T_{min}, T_{max}, then $\mu_{i,LB}(T) < 0$ for T in the interval $[T_{min}, T_{max}]$ and $\mu_{i,LB}(T) > 0$ otherwise. Moreover, $\mu_{i,c} < 0$ (by definition), so $\mu_{i,LB}(0) < 0$ and thus $0 \in [T_{min}, T_{max}]$. The condition for positive μ_i along the trajectory is then

$$T > T_{i,max} = \frac{-\mu_{i,T} + \sqrt{\mu_{i,T}^2 - 4\mu_{i,T^2}\mu_{i,c}}}{2\mu_{i,T^2}} \tag{42}$$

Finally, the sufficient (albeit not necessary) condition on T to ensure feasibility is

$$T > \max\left\{T_{1,max}, T_{2,max}, T_{3,max}\right\} \tag{43}$$

The strategy defined above has a drawback in the limit cases where $\omega = \omega_{min}$ or $\omega = \omega_{max}$ (with ω_{min}, ω_{max} defined as in eq. (27)). In such cases we have respectively $\omega^2 = w_{i,min}$ or $\omega^2 = w_{i,max}$, for one $i \in \{1,2,3\}$: the corresponding μ_i has then minimum value $\mu_{i,2} = 0$. When this happens, at least one of the cable tensions τ_i reaches zero at some point, while being still greater than zero along the rest of the trajectory.

However, if $\mu_{i,0,LB} = \mu_{i,2} = 0$, there are no finite values of T that make $\mu_{i,LB} > 0$ (as defined in eq. (40)), since all terms on the right side are negative, except for $\mu_{i,0,LB}$, which is zero. As ω gets close to the limits ω_{min}, ω_{max} of the admissible range, at least one of the $T_{i,max}$ approaches $+\infty$ (see eq. (42), where $\mu_{i,T^2} = \mu_{i,0,LB} \to 0$).

Note that having T approaching $+\infty$ is a mathematical consequence of the conditions found in eq. (43), which are sufficient but not strictly necessary. The actual minimum value of T that makes a given transition trajectory feasible has been numerically found in a series of computational experiments and compared with the minimum defined in eq. (43): we found that T is acceptably close to the actual minimum when ω is close to the middle of the admissible range $[\omega_{min}, \omega_{max}]$. When instead ω is close to the limits of the range, the minimum value of T to ensure feasibility remains bounded, while the lower bound defined by eq. (43) goes to infinity. This limit can be circumvented in practice by using the frequency changing method introduced in Section 5: we may choose an ω which is roughly in the middle of the admissible range for the corresponding elliptical trajectory Γ, move the robot from a rest condition to Γ using the transition trajectory just outlined, and finally change the frequency ω to the desired value, using the method presented in Section 5.

It is worth noting that the special case $\omega_{min} = 0$ can only happen when Γ is entirely within the SEW (see Section 4). In such a case, the three $w_{i,min}$ in eq. (27) are negative, μ_{i,T^2} from eq. (42) is positive and the three $T_{i,max}$ remain bounded even if $\omega \to \omega_{min}$. This case has little practical interest.

6.2 Variable centre

In this subsection, we study the possibility of moving the ellipse centre. We define a new transition trajectory, based on the original one shown in eq. (1), as follows:

$$\mathbf{p} = \left[\mathbf{p}_{C,s} + U(\xi)\mathbf{p}_{sf}\right] + \mathbf{p}_d \tag{44}$$

with $\mathbf{p}_d$ as in Section 2 (where $\psi = \omega t$ and ω is a constant frequency) and $U(\xi)$ being a function of class C^2 in the variable $\xi = t/T$, where T is the duration of the transition.

This is a further generalization of eq. (1) and allows to smoothly connect two elliptical trajectories Γ_s and Γ_f having the same shape and orientation, but different centres $\mathbf{p}_{C,s}$ and $\mathbf{p}_{C,f}$, with $\mathbf{p}_{sf} = \mathbf{p}_{C,f} - \mathbf{p}_{C,s} = \left[x_{sf}, y_{sf}, z_{sf}\right]^T$.

In order to do this, we have to set the boundary conditions seen in eq. (33) and require $V(\xi)$ to be positive for any value of ξ, as we already did for the variable amplitudes transition motion (Subsection 6.1).

Substituting the trajectory equation (44) in the conditions (13), we obtain (after some simplification)

$$\mu_i = \mu_{i,s} + U(\xi)(\mu_{i,f} - \mu_{i,s}) + \frac{W(\xi)}{T^2} q_{i,sf} \tag{45}$$

Here, we introduce the variables:

$$\begin{aligned} \mathbf{v}_{Ci,s} &= \mathbf{a}_i - \mathbf{p}_{C,s} \\ \boldsymbol{\lambda}_{i,s} = [\lambda_{xi,s}, \lambda_{yi,s}, \lambda_{zi,s}]^T &= \mathbf{v}_{Cj,s} \times \mathbf{v}_{Ck,s} \\ \boldsymbol{\lambda}_{i,f} = [\lambda_{xi,f}, \lambda_{yi,f}, \lambda_{zi,f}]^T &= \mathbf{v}_{Cj,f} \times \mathbf{v}_{Ck,f} \\ q_{i,sf} &= (\mathbf{p}_d \times \mathbf{v}_{jk} - \boldsymbol{\lambda}_{i,s}) \cdot \mathbf{p}_{sf} \end{aligned} \tag{46}$$

$\mu_{i,f}$ and $\mu_{i,s}$ are functions of time and are defined as per eqs. (20)-(22), with $\dot{\psi} = \omega$ and $\ddot{\psi} = 0$; here, however, we replace $\lambda_{xi}, \lambda_{yi}, \lambda_{zi}$ in eq. (22) respectively with $\lambda_{xi,f}, \lambda_{yi,f}, \lambda_{zi,f}$ and $\lambda_{xi,s}, \lambda_{yi,s}, \lambda_{zi,s}$. With these definitions, $\mu_{i,f}$ and $\mu_{i,s}$ correspond to μ_i for the start and target trajectories Γ_s and Γ_f.

If we now consider eq. (45) and let $T \to \infty$, then $\mu_i \to \mu_{i,s} + U(\xi)(\mu_{i,f} - \mu_{i,s})$; since we asked $U(\xi)$ to be monotonically increasing from 0 to 1, then $\mu_i \in \left[\mu_{i,s}, \mu_{i,f}\right] \ \forall t$. If Γ_s and Γ_f are both feasible, then $\mu_{i,s} \geq \mu_{i,2,s} \geq 0$ and $\mu_{i,f} \geq \mu_{i,2,f} \geq 0$, again $\forall t$; we can then safely conclude that $\mu_i \geq \min\left\{\mu_{i,2,s}, \mu_{i,2,f}\right\} \geq 0$. We can thus say that if the transition trajectory defined by eq. (44) connects two ellipses that are feasible, as long as T is large enough.

At this point we want to find a lower bound on T such that the transition is feasible. As in Subsection 6.1, finding the minimum feasible value T is a complex task that cannot be analytically solved; however, defining a safe lower bound is enough for practical purposes.

For this we reconsider eq. (45), specifically the second term $W(\xi)/T^2 q_{i,sf}$: this is the term that may become negative along the trajectory. We introduce the upper and lower extrema of $W(\xi)$ as W_{max} and W_{min}; these are known from the choice of the transition motion $U(\xi)$. We note that, in general, for any function $U(\xi)$ of class C^2 that satisfies the boundary conditions in eq. (33) it will hold that $W_{min} < 0, W_{max} > 0$. It can then be proved the following:

$$\begin{aligned} \min\left\{W(\xi) q_{i,sf}\right\} \geq \min\big\{ & W_{min} \cdot \max\left\{q_{i,sf}\right\}, \\ & W_{max} \cdot \min\left\{q_{i,sf}\right\} \big\} \end{aligned} \tag{47}$$

From the definition in eq. (46), $q_{i,sf}$ is a trigonometric function of time (having frequency ω) that can be written as

$$\begin{aligned} q_{i,sf} &= C_{i,sf}\cos(\omega t) + D_{i,sf}\sin(\omega t) + E_{i,sf} \\ C_{i,sf} &= (\mathbf{p}_{d,s} \times \mathbf{v}_{jk}) \cdot \mathbf{p}_{sf} \\ D_{i,sf} &= (\mathbf{p}_{d,c} \times \mathbf{v}_{jk}) \cdot \mathbf{p}_{sf} \\ E_{i,sf} &= -\boldsymbol{\lambda}_{i,s} \cdot \mathbf{p}_{sf} \end{aligned} \tag{48}$$

In this expression, the coefficients $C_{i,sf}$, $D_{i,sf}$ and $E_{i,sf}$ are constant; it then follows that the extrema of $q_{i,sf}$ are

$$\begin{aligned} \max\left\{q_{i,sf}\right\} &= E_{i,sf} + \sqrt{C_{i,sf}^2 + D_{i,sf}^2} \\ \min\left\{q_{i,sf}\right\} &= E_{i,sf} - \sqrt{C_{i,sf}^2 + D_{i,sf}^2} \end{aligned} \tag{49}$$

(cf. eq. (23)). Going back to eq. (45), we can now write its lower bound as

$$\mu_{i,LB}(T) = \frac{\mu_{i,c} + \mu_{i,T^2} T^2}{T^2} = \frac{M_i(T)}{T^2} \leq \mu_i \tag{50}$$

with

$$\begin{aligned} \mu_{i,c} &= \min\left\{W(\xi) q_{i,sf}\right\} \ \leq 0 \\ \mu_{i,T^2} &= \min\left\{\mu_{i,2,s}, \mu_{i,2,f}\right\} \geq 0 \end{aligned} \tag{51}$$

which replace eqs. (40) and eq. (41). We can be sure that $\mu_{i,T^2} \geq 0$ if the ellipses Γ_s and Γ_f are feasible; the fact that $\mu_{i,c} \leq 0$ can be inferred by observing that in eq. (47) at least one of the two terms is negative, since $W_{min} < 0$, $W_{max} > 0$ and clearly $\min\left\{q_{i,sf}\right\} < \max\left\{q_{i,sf}\right\}$.

The considerations in Subsection 6.1 then apply: $\mu_{i,LB}(T) < 0$ if and only if T is in the interval $[T_{min}, T_{max}]$ (with T_{min}, T_{max} being the solutions of $M_i(T) = 0$), since the coefficient μ_{i,T^2} of the quadratic term in $M_i(T)$ is positive; also, $\mu_{i,LB}(0) = \mu_{i,c} \leq 0$, so $0 \in [T_{min}, T_{max}]$. The condition for positive μ_i along the trajectory is then

$$T > T_{i,max} = \sqrt{-\frac{\mu_{i,c}}{\mu_{i,T^2}}} \tag{52}$$

We may conclude that a sufficient condition to have positive tensions in the cables along the transition motion is given by eq. (43), with $T_{i,max}$ given by eq. (52).

Note that, if the start and target elliptical trajectories have to be feasible, then it must hold that $\omega \in \left[\omega_{min,s}, \omega_{max,s}\right] \cap \left[\omega_{min,f}, \omega_{max,f}\right] = \left[\omega_{min,sf}, \omega_{max,sf}\right]$, namely, the frequency ω along the transition motion must be in the ranges of admissible frequencies both for Γ_s and Γ_f; clearly here we have to assume that such ranges overlap, otherwise there are no values of ω such that both ellipses are feasible.

As seen in Subsection 6.1, some issues arise when ω is close to the boundaries $\omega_{min,sf}$ or $\omega_{max,sf}$ of the admissible range (given by the intersection of the start and the end range). For example, $\omega = \omega_{min,sf}$ means either $\omega^2 = w_{i,s,min}$ or $\omega^2 = w_{i,f,min}$, for some $i \in \{1,2,3\}$ (with $w_{i,s,min}$ and $w_{i,f,min}$ being the values given by eq. (26), for the start and the target ellipse). In such a case, the corresponding μ_{i,T^2} from eq. (51) is zero, since either $\mu_{i,2,f} = 0$ or $\mu_{i,2,f} = 0$, and $T_{i,max}$ is not defined. Again, this is a consequence of using a sufficient, but not strictly necessary condition; the actual minimum value of T remains finite even as $\omega \to \omega_{min,sf}$. Analogous considerations hold for $\omega \to \omega_{max,sf}$. The special case $\omega_{min,sf} = 0$ can happen only if both Γ_s and Γ_f are within the SEW and has little practical interest.

To conclude this section on transition trajectories, we remark that, if the frequency ω of the transition motion (for either the case of variable amplitude or the case of variable centre) can be chosen freely, a reasonable approach is to pick $\omega \approx (\omega_{min} + \omega_{max})/2$, with $\omega_{min}, \omega_{max}$ being the lower and upper endpoints of the range of admissible frequencies. In this way, we are farthest from the endpoints and we may expect the transition time to be close to the actual minimum.

If instead we have to connect two (feasible) elliptical trajectories Γ_s and Γ_f, with assigned frequencies ω_s and ω_f, we can combine the transition motions described in this section with the method shown in Section 5 to vary the motion frequency. For example, consider two ellipses Γ_s and Γ_f having the same shape and orientation, but different centres $\mathbf{p}_{C,s}$ and $\mathbf{p}_{C,f}$. Assume that the admissible range of frequencies for Γ_s, $\left[\omega_{min,s}, \omega_{max,s}\right]$, overlaps with the admissible range for Γ_f, $\left[\omega_{min,f}, \omega_{max,f}\right]$; Γ_s has to be followed with frequency $\omega_s \in \left[\omega_{min,s}, \omega_{max,s}\right]$ and Γ_f with frequency $\omega_f \in \left[\omega_{min,f}, \omega_{max,f}\right]$ (where in general $\omega_s \neq \omega_f$). An approach to smoothly connect the start and the target trajectory could be divided in three steps, as follows:

- first, we change the frequency along Γ_s, from ω_s to $\omega_{sf} \in \left[\omega_{min,s}, \omega_{max,s}\right] \cap \left[\omega_{min,f}, \omega_{max,f}\right] = \left[\omega_{min,sf}, \omega_{max,sf}\right]$; a good approach would be to take $\omega_{sf} \approx \left(\omega_{min,sf} + \omega_{max,sf}\right)/2$.
- then we move along the variable-centre transition motion defined in Subsection 6.2, with constant frequency ω_{sf};
- finally, we change the frequency again, moving along Γ_f, from ω_{sf} to ω_f.

Should the admissible frequency ranges for Γ_s and Γ_f have no overlap, we could find an intermediate ellipse Γ_i whose admissible range has a nonempty intersection with the admissible ranges for both the start and the end ellipse and then repeat the steps defined above to smoothly connect Γ_s with Γ_i, and Γ_i with Γ_f.

By suitably combining the various motion types described in the previous sections, a great variety of dynamic trajectories can be obtained.

7 Experimental results

To validate our theoretical results, we also performed a series of tests on the CSPR prototype in the Laboratoire de Robotique at Université Laval. The results of the experiments can be found in the multimedia attachments, where the robot performs the dynamic trajectories presented here: as can be seen in the video, the robot is clearly moving outside the SEW while keeping positive tensions in the cables. In parts of the trajectory, however, one or more cables start vibrating: this is due to the limitations of the prototype, since the end-effector has finite dimensions and the cable attachment points on it do not coincide, so that the point-mass model approximation has limited validity and the end-effector rotates around its centre

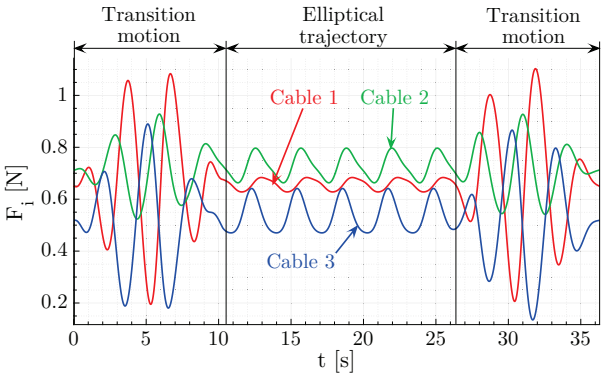

Fig. 5: Cable tensions along a spatial trajectory.

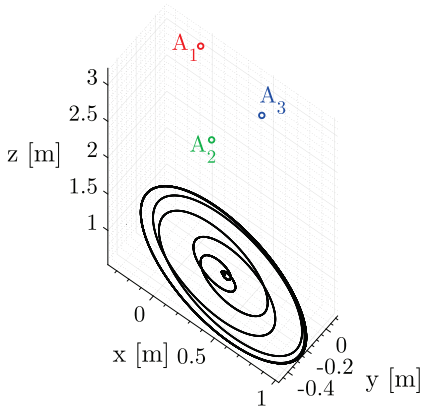

Fig. 6: Trajectory of the robot during the experiments (first part in attached video, simple periodic elliptical trajectory).

of mass; in any case, we found that the desired trajectories were followed reasonably well.

The first trajectory shown in the video is a simple ellipse with constant frequency (see Section 4). The robot starts moving with growing amplitudes of oscillation, by using the transition motion described in Subsection 6.1; it then reaches the target elliptical trajectory which clearly goes outside the SEW, on which it keeps moving before slowing down and going back to a rest condition within the SEW (see Fig. 5). The 3D depiction of the trajectory is shown in Fig. 6.

After that, the robot performs the variable frequency trajectory described in Section 5. The robot starts moving with a given frequency $\omega = \omega_{med}$ along a given ellipse, then accelerates and moves with a higher frequency $\omega = \omega_{sup}$, so that it is moving at higher velocities (while remaining on the same ellipse). After that, the frequency is lowered to $\omega = \omega_{inf}$; finally, the frequency is changed again to ω_{med}. Clearly, it must hold $\omega_{min} < \omega_{inf} < \omega_{med} < \omega_{sup} < \omega_{max}$ for the trajectory to be feasible, where $\omega_{min}, \omega_{max}$ are those given by (27). It is to be noted that this trajectory, too, moves outside the SEW, although this is difficult to notice due to the perspective in the video.

Finally, the third video shows the transition trajectories defined in Section 6. Again, the robot starts moving with a variable amplitudes trajectory from a rest position in the SEW until it reaches a target upper trajectory. After that, the variable centre transition from Subsection 6.2 is applied, so the robot moves now on a lower trajectory. Finally, the dynamic motion is stopped, again by using a variable amplitude motion.

The control system of the prototype provides the cable length at every timestep, by using the motor rotations measured by the encoders: by comparing the actual lengths to the desired values set as targets, we found an average error over the entire motion of about 4.4×10^{-2} mm and a maximum value of 1 mm. By solving the direct kinematic problem, we found that the corresponding average and maximum errors in 3D space are respectively 9.5×10^{-1} mm and 7.3 mm: given that the workspace dimensions are in the order of meters, these errors can be acceptable.

8 Conclusions

In this paper we defined a general class of periodic elliptical trajectories for a cable-suspended parallel robot (CSPR), modeled as a point-mass end-effector suspended by three cables. The robot position can be properly controlled, with positive tensions in the cables, even as it moves beyond its static workspace.

Furthermore, we defined transition trajectories to perform one of the following:

- change the frequency with which a given ellipse is followed (so as to increase or reduce the motion velocity);
- move the robot from a state of rest to one of the aforementioned periodic trajectories, or vice versa;
- smoothly connect two elliptical trajectories having the same shape, orientation and centre, but different sizes;
- smoothly connect two elliptical trajectories having the same shape, orientation and size, but different centres.

For all aforementioned trajectories we found conditions for feasibility: the conditions for the periodic trajectories are necessary and sufficient, whereas the conditions for the transition motions are only sufficient. All conditions are algebraic inequalities that can be verified in a few milliseconds; this makes the proposed work applicable for real-time problems.

The trajectories shown in this paper expand and generalize previous results [1], [18], [23], [24]. One of the advantages of the proposed trajectories is that there are many parameters that can be chosen; therefore, they provide greater flexibility during the trajectory planning phase.

Future plans include studying how to combine multiple ellipses or elliptical arcs in piecewise trajectories, in order to provide more general dynamic point-to-point motions for CSPRs; this would generalize the works in [20], [21].

Acknowledgment

The authors would like to thank Dr. Xiaoling Jiang for her insightful remarks on earlier versions of this paper, Mr. Simon Foucault for his help on the experimental part and Mr. André Gallant for his help on the video editing.

References

[1] Mottola, G., Gosselin, C., and Carricato, M., 2018. "Dynamically feasible elliptical trajectories for fully constrained 3-dof cable-suspended parallel robots". In *Cable-Driven Parallel Robots*, C. Gosselin, P. Cardou, T. Bruckmann, and A. Pott, eds. Springer International Publishing, Québec, Canada, pp. 221–230.

[2] Riechel, A. T., and Ebert-Uphoff, I., 2004. "Force-feasible workspace analysis for underconstrained point-mass cable robots". In IEEE Int. Conf. on Robotics and Automation, New Orleans, USA, pp. 4956–4962.

[3] Barrette, G., and Gosselin, C., 2005. "Determination of the dynamic workspace of cable-driven planar parallel mechanisms". *ASME J. Mech. Design,* **127**(2), pp. 242–248.

[4] Carricato, M., and Merlet, J.-P., 2013. "Stability analysis of underconstrained cable-driven parallel robots". *IEEE Trans. Robot.,* **29**(1), pp. 288–296.

[5] Berti, A., Merlet, J.-P., and Carricato, M., 2016. "Solving the direct geometrico-static problem of underconstrained cable-driven parallel robots by interval analysis". *Int. J. Robot. Research,* **35**(6), pp. 723–739.

[6] Abbasnejad, G., and Carricato, M., 2015. "Direct geometrico-static problem of underconstrained cable-driven parallel robots with *n* cables". *IEEE Trans. Robot.,* **31**(2), pp. 468–478.

[7] Cunningham, D., and Asada, H. H., 2009. "The winchbot: A cable-suspended, under-actuated robot utilizing parametric self-excitation". In IEEE Int. Conf. on Robotics and Automation, Kobe, Japan, pp. 1844–1850.

[8] Lefrancois, S., and Gosselin, C., 2010. "Point-to-point motion control of a pendulum-like 3-dof underactuated cable-driven robot". In IEEE Int. Conf. on Robotics and Automation, Anchorage, USA, pp. 5187–5193.

[9] Zoso, N., and Gosselin, C., 2012. "Point-to-point motion planning of a parallel 3-dof underactuated cable-suspended robot". In IEEE Int. Conf. on Robotics and Automation, Saint Paul, USA, pp. 2325–2330.

[10] Zanotto, D., Rosati, G., and Agrawal, S. K., 2011. "Modeling and control of a 3-dof pendulum-like manipulator". In IEEE Int. Conf. on Robotics and Automation, Shanghai, P.R.C., pp. 3964–3969.

[11] Idá, E., Berti, A., Bruckmann, T., and Carricato, M., 2018. "Rest-to-rest trajectory planning for planar underactuated cable-driven parallel robots". In *Cable-Driven Parallel Robots*, C. Gosselin, P. Cardou, T. Bruckmann, and A. Pott, eds. Springer International Publishing, Québec, Canada, pp. 207–218.

[12] Barbazza, L., Zanotto, D., Rosati, G., and Agrawal, S. K., 2017. "Design and optimal control of an underactuated cable-driven micro-macro robot". *IEEE Robot. Autom. Lett.,* **2**(2), pp. 896–903.

[13] Bamdad, M., Taheri, F., and Abtahi, N., 2015. "Dynamic analysis of a hybrid cable-suspended planar manipulator". In IEEE Int. Conf. on Robotics and Automation, Seattle, USA, pp. 1621–1626.

[14] Trevisani, A., 2010. "Underconstrained planar cable-direct-driven robots: A trajectory planning method ensuring positive and bounded cable tensions". *Mechatronics,* **20**, pp. 113–127.

[15] Trevisani, A., 2013. "Planning of dynamically feasible trajectories for translational, planar, and underconstrained cable-driven robots". *Journal of Systems Science and Complexity,* **26**(5), pp. 695–717.

[16] Trevisani, A., 2012. "Experimental validation of a trajectory planning approach avoiding cable slackness and excessive tension in underconstrained translational planar cable-driven robots". In *Cable-Driven Parallel Robots*, T. Bruckmann and A. Pott, eds. Springer-Verlag Berlin Heidelberg, Stuttgart, Germany, pp. 23–39.

[17] Gosselin, C., Ren, P., and Foucault, S., 2012. "Dynamic trajectory planning of a two-dof cable-suspended parallel robot". In 2012 IEEE Int. Conf. on Robotics and Automation, Saint Paul, USA, pp. 1476–1481.

[18] Gosselin, C., 2012. "Global planning of dynamically feasible trajectories for three-dof spatial cable-suspended parallel robots". In *Cable-Driven Parallel Robots*, T. Bruckmann and A. Pott, eds. Springer-Verlag Berlin Heidelberg, Stuttgart, Germany, pp. 3–22.

[19] Jiang, X., and Gosselin, C., 2014. "Dynamically feasible trajectories for three-dof planar cable-suspended parallel robots". In ASME Int. Design Tech. Conf., Buffalo, USA.

[20] Gosselin, C., and Foucault, S., 2014. "Dynamic point-to-point trajectory planning of a two-dof cable-suspended parallel robot". *IEEE Trans. Robot.,* **30**(3), June, pp. 728–736.

[21] Jiang, X., and Gosselin, C., 2016. "Dynamic point-to-point trajectory planning of a three-dof cable-suspended parallel robot". *IEEE Trans. Robot.,* **32**(6), pp. 1550–1557.

[22] Liang, D., Song, Y., and Sun, T., 2017. "Nonlinear dynamic modeling and performance analysis of a redundantly actuated parallel manipulator with multiple actuation modes based on fmd theory". *Nonlinear dynamics,* **89**(1), pp. pp. 391–428.

[23] Zhang, N., and Shang, W., 2016. "Dynamic trajectory planning of a 3-dof under-constrained cable-driven parallel robot". *Mech. Mach. Theory,* **98**, pp. 21–35.

[24] Zhang, N., Shang, W., and Cong, S., 2016. "Geometry-based trajectory planning of a 3-3 cable-suspended parallel robot". *IEEE Trans. Robot.,* **33**(2), pp. pp. 484–491.

[25] Berti, A., Gouttefarde, M., and Carricato, M., 2016. "Dynamic recovery of cable-suspended parallel robots after a cable failure". In *Advances in Robot Kinematics*, J. Lenarcic and J.-P. Merlet, eds. Springer International Publishing, Grasse, France, pp. 337–344.

[26] Schmidt, V., Kraus, W., Ho, W. Y., Seon, J., Pott, A., Park, J., and Verl, A., 2014. "Extending dynamic trajectories of cable-driven parallel robots as a novel robotic roller coaster". In 41st Int. Symp. Robotics, Munich, Germany, pp. 367–373.

Appendices

A Proof that any ellipse can be written as in Section 2.

Let $x'y'$ be a coordinate plane with origin O' in the centre C of the ellipse and the coordinate axes directed along the principal axes. The parametric equations of the ellipse in plane $x'y'$ are

$$\mathbf{p}' = \begin{bmatrix} x' \\ y' \\ z' \end{bmatrix} = \begin{bmatrix} A\cos(\psi) \\ B\sin(\psi) \\ 0 \end{bmatrix} \tag{53}$$

with A, B being the semimajor and semiminor axes.

If we now apply the coordinate transformation $\mathbf{p} = \mathbf{R}\mathbf{p}' + \mathbf{p}_C$, where $\mathbf{R} = (r_{ij}) \in \mathbb{R}^{3\times3}$ is the rotation matrix from $O'x'y'z'$ to $Oxyz$ and $\mathbf{p}_C = [x_C, y_C, z_C]^T$ is the position vector of C in $Oxyz$, we still obtain an ellipse, since this transformation corresponds to a rigid motion. From eq. (53) the x coordinate can be expanded as

$$x = r_{11}A\cos(\psi) + r_{12}B\sin(\psi) + x_C \tag{54}$$

We can now define an amplitude x_A and a phase angle ϕ_x as

$$\begin{aligned} x_A &= \sqrt{r_{11}^2A^2 + r_{12}^2B^2} \\ \phi_x &= \operatorname{atan}_2\left(\frac{r_{11}A}{x_A}, \frac{r_{12}B}{x_A}\right) \end{aligned} \tag{55}$$

and, by dividing eq. (54) by x_A, we obtain

$$\begin{aligned} x &= x_A\left[\frac{r_{11}A}{x_A}\cos(\omega t) + \frac{r_{12}B}{x_A}\sin(\omega t)\right] + x_C \\ &= x_A\left[\sin(\phi_x)\cos(\omega t) + \cos(\phi_x)\sin(\omega t)\right] + x_C \\ &= x_A\sin(\omega t + \phi_x) + x_C \end{aligned} \tag{56}$$

which is equivalent to the expression for x given by eq. (1); the same proof applies for the y and z coordinates. Note that, by following the same steps backwards, we can also show that all trajectories defined by eq. (1) are indeed ellipses.

B Proof of properties in Section 5

First, it is useful to prove that

$$C_{i,v}D_{i,c} - C_{i,c}D_{i,v} = E_{i,a}E_{i,c} \tag{57}$$

This can be seen by substituting the definitions in eq. (22) into eq. (57); one finds, after some simplification,

$$\begin{aligned} &C_{i,v}D_{i,c} - C_{i,c}D_{i,v} - E_{i,a}E_{i,c} \\ &= -gx_Ay_A(\mathbf{v}_{kj}\cdot\boldsymbol{\lambda}_i)\sin(\phi_{xy}) \\ &= -gx_Ay_A[\mathbf{v}_{kj}\cdot(\mathbf{v}_{Cj}\times\mathbf{v}_{Ck})]\sin(\phi_{xy}) \end{aligned} \tag{58}$$

where in the last identity we used the definition of $\boldsymbol{\lambda}_i$ from eq. (4). Now, looking at the definitions in eq. (2) and eq. (3), we see that the three vectors $\mathbf{v}_{kj} = \mathbf{a}_j - \mathbf{a}_k$, $\mathbf{v}_{Cj} = \mathbf{a}_j - \mathbf{p}_C$ and $\mathbf{v}_{Ck} = \mathbf{a}_k - \mathbf{p}_C$ are all contained in the same plane, passing through points C, A_j and A_k: thus, the triple vector product $\mathbf{v}_{kj}\cdot(\mathbf{v}_{Cj}\times\mathbf{v}_{Ck})$ is zero, which proves eq. (57).

If we now substitute eq. (25) into $\Delta_i = \beta_i^2 - \alpha_i\gamma_i$ as defined in Section 4 and simplify, we obtain

$$\begin{aligned} \Delta_i &= (C_{i,v}^2 + D_{i,v}^2)E_{i,c}^2 - (C_{i,v}D_{i,c} - C_{i,c}D_{i,v})^2 \\ &= (C_{i,v}^2 + D_{i,v}^2 - E_{i,a}^2)E_{i,c}^2 = \gamma_{i,\ddot{\psi}}E_{i,c}^2 \end{aligned} \tag{59}$$

where in the last step we used eq. (57). If the centre C of the elliptical trajectory under consideration is in the SEW, then $\Delta_i > 0$ (see Section 4) and thus $\gamma_{i,\ddot{\psi}} = C_{i,v}^2 + D_{i,v}^2 - E_{i,a}^2 > 0$.

To prove that Ω_i is an ellipse in the $\ddot{\psi} - w$ plane, we consider its boundary, as defined by $\alpha_i w^2 + 2\beta_i w + \gamma_i'(\ddot{\psi}) = \alpha_i w^2 + 2\beta_i w + \ddot{\psi}^2\gamma_{i,\ddot{\psi}} + \gamma_i = 0$. This is a quadratic curve in the $\ddot{\psi} - w$ plane; to verify that it is an ellipse, we first define

$$\begin{aligned} \Delta_{\Omega,i} &= \begin{vmatrix} \gamma_{i,\ddot{\psi}} & 0 & 0 \\ 0 & \alpha_i & \beta_i \\ 0 & \beta_i & \gamma_i \end{vmatrix} \\ J_{\Omega,i} &= \begin{vmatrix} \gamma_{i,\ddot{\psi}} & 0 \\ 0 & \alpha_i \end{vmatrix} \\ I_{\Omega,i} &= \gamma_{i,\ddot{\psi}} + \alpha_i \end{aligned} \tag{60}$$

As known from plane geometry, Ω_i is an ellipse if and only if $\Delta_{\Omega,i} \neq 0$, $J_{\Omega,i} > 0$ and $\Delta_{\Omega,i}/I_{\Omega,i} < 0$. It is easy to see that $\Delta_{\Omega,i} = \gamma_{i,\ddot{\psi}}(\alpha_i\gamma_i - \beta_i^2) = -\gamma_{i,\ddot{\psi}}\Delta_i < 0$ since we assumed that the centre of the trajectory is in the SEW, so that $\Delta_i > 0$ and consequently $\gamma_{i,\ddot{\psi}} > 0$.

Assume first $\alpha_i > 0$: in this case $J_{\Omega,i} = \gamma_{i,\ddot{\psi}}\alpha_i > 0$ and also $I_{\Omega,i} > 0$, so the conditions that define an ellipse are fulfilled.

If instead $\alpha_i = 0$ (remember that $\alpha_i \geq 0$), then $\beta_i = 0$, as stated in Section 4. Also, recall that in this case the trajectory is contained in the plane through points C, A_j and A_k, so $E_{i,a} = \mathbf{v}_{kj}\cdot\mathbf{n}_e = 0$ since $\mathbf{v}_{kj} = \mathbf{a}_j - \mathbf{a}_k$ is contained in this plane while $\mathbf{n}_e$ is the vector normal to the plane containing the trajectory. Thus, $\gamma_{i,\ddot{\psi}} = C_{i,v}^2 + D_{i,v}^2 - E_{i,a}^2 = \alpha_i - E_{i,a}^2 = 0$ and the condition that defines Ω_i degenerates to $\gamma_i < 0$: if this condition is satisfied, then Ω_i coincides with the whole plane $\ddot{\psi} - w$.

When $\ddot{\psi}$ becomes large enough, the admissible range of w degenerates into a single point; this happens for

$$\ddot{\psi}^2 = \ddot{\psi}_{i,e}^2 = \Delta_i/(\alpha_i\gamma_{i,\ddot{\psi}}) \tag{61}$$

as can be seen by setting $\Delta_i' = \Delta_i - \alpha_i\ddot{\psi}^2\gamma_{i,\ddot{\psi}} = 0$ and solving for $\ddot{\psi}^2$. The admissible area Ω_i is then contained within the limits $-\ddot{\psi}_{i,e} < \ddot{\psi} < \ddot{\psi}_{i,e}$.

We previously required (in Section 5) that $E_i > 0$; we can now show that this is in fact the case for every point in Ω_i.

Indeed, from eq. (21) we get

$$E_i = E_{i,a}\ddot{\psi}^2 + E_{i,c} > 0 \Rightarrow \begin{cases} \ddot{\psi} > \ddot{\psi}_{i,l},\ E_{i,a} > 0 \\ \ddot{\psi} < \ddot{\psi}_{i,l},\ E_{i,a} < 0 \end{cases} \tag{62}$$

with

$$\ddot{\psi}_{i,l} = -E_{i,c}/E_{i,a}, \quad \begin{cases} \ddot{\psi}_{i,l} < 0, & E_{i,a} > 0 \\ \ddot{\psi}_{i,l} > 0, & E_{i,a} < 0 \end{cases} \tag{63}$$

where we have used $E_{i,c} = \lambda_{zi} g > 0$ when C is in the SEW (see Section 3). From this we find that if $|\ddot{\psi}| < |\ddot{\psi}_{i,l}|$ then $E_i > 0$, as desired. However, Ω_i is strictly contained in the range thus found, since $|\ddot{\psi}_{i,e}| < |\ddot{\psi}_{i,l}|$. This is seen by squaring both sides of the inequality and using the definitions from eqs. (61) and (63):

$$\ddot{\psi}_{i,e}^2 < \ddot{\psi}_{i,l}^2 \Rightarrow \frac{\gamma_{i,\ddot{\psi}} E_{i,c}^2}{\gamma_{i,\ddot{\psi}} \left(C_{i,v}^2 + D_{i,v}^2 \right)} < \frac{E_{i,c}^2}{E_{i,a}^2} \tag{64}$$

where we have used the equivalent definition of Δ_i from eq. (59) and the definition of α_i from eq. (25). After simplification, this finally reduces to $C_{i,v}^2 + D_{i,v}^2 - E_{i,a}^2 = \gamma_{i,\ddot{\psi}} > 0$, which has already been proved.

C Proof of properties in Subsection 6.1

To find the extreme values of $q_{i,W}$ and $q_{i,V}$, which depend on t, we remember that a sinusoidal function having frequency ω can be seen as the projection along a fixed line of a phase vector rotating with angular velocity ω. Note that $q_{i,W}$ and $q_{i,V}$ from Subsection 6.1 are defined respectively as sums of sinusoidal and cosinusoidal functions (see eq. (35), where $\boldsymbol{\lambda}_i$ is a constant vector and $\mathbf{p}_d$, $\dot{\mathbf{p}}_d$ from eq. (1) are respectively a sine and a cosine function of time t). Thus, they can be expressed as the projections of a rotating phase vector $\boldsymbol{\Phi}_i$ along two orthogonal axes (here it's convenient to consider $q_{i,V}/(2\omega)$ instead of $q_{i,V}$ for dimensional homogeneity), with $\boldsymbol{\Phi}_i = \boldsymbol{\Phi}_{x,i} + \boldsymbol{\Phi}_{y,i} + \boldsymbol{\Phi}_{z,i}$ (see Fig. 7) and where such vectors have the following magnitudes and phases:

$$\begin{aligned} \|\boldsymbol{\Phi}_{x,i}\| &= |x_A \lambda_{xi}|, \angle\boldsymbol{\Phi}_{x,i} = \phi_x + \pi/2[1 + \mathrm{sgn}(\lambda_{xi})] \\ \|\boldsymbol{\Phi}_{y,i}\| &= |y_A \lambda_{yi}|, \angle\boldsymbol{\Phi}_{y,i} = \phi_y + \pi/2[1 + \mathrm{sgn}(\lambda_{yi})] \\ \|\boldsymbol{\Phi}_{z,i}\| &= |z_A \lambda_{zi}|, \angle\boldsymbol{\Phi}_{z,i} = \phi_z + \pi/2[1 + \mathrm{sgn}(\lambda_{zi})] \end{aligned} \tag{65}$$

Then we have $q_{i,V}/(2\omega) = \|\boldsymbol{\Phi}_i\| \cos(\angle\boldsymbol{\Phi}_i + \omega t)$ and $q_{i,W} = \|\boldsymbol{\Phi}_i\| \sin(\angle\boldsymbol{\Phi}_i + \omega t)$, which can be verified by substitution. From this the extrema in eq. (36) are proved.

The components of $\boldsymbol{\Phi}_i$, in the $q_{i,V}/(2\omega) - q_{i,W}$ plane, are respectively $\|\boldsymbol{\Phi}_{x,i}\| \cos(\angle\boldsymbol{\Phi}_{x,i}) + \|\boldsymbol{\Phi}_{y,i}\| \cos(\angle\boldsymbol{\Phi}_{y,i}) + \|\boldsymbol{\Phi}_{z,i}\| \cos(\angle\boldsymbol{\Phi}_{z,i})$ and $\|\boldsymbol{\Phi}_{x,i}\| \sin(\angle\boldsymbol{\Phi}_{x,i}) + \|\boldsymbol{\Phi}_{y,i}\| \sin(\angle\boldsymbol{\Phi}_{y,i}) + \|\boldsymbol{\Phi}_{z,i}\| \sin(\angle\boldsymbol{\Phi}_{z,i})$; these are respectively $C_{i,a}$ and $D_{i,a}$, which again can be found by substitution. This proves eq. (37).

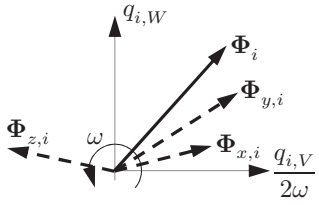

Fig. 7: The vectors $\boldsymbol{\Phi}_{x,i}$, $\boldsymbol{\Phi}_{y,i}$ and $\boldsymbol{\Phi}_{z,i}$, with their sum $\boldsymbol{\Phi}_i$, rotate in the $q_{i,V}/(2\omega) - q_{i,W}$ plane at angular velocity ω.

List of Figures